HHS Public Access

Author manuscript

Inhal Toxicol. Author manuscript; available in PMC 2015 December 01.

Published in final edited form as:

Inhal Toxicol. 2014 February ; 26(2): 70–83. doi:10.3109/08958378.2013.854851.

Efficacy of screens in removing long fibers from an aerosol stream – sample preparation technique for toxicology studies

Bon Ki Ku, **Gregory J. Deye**, and **Leonid A. Turkevich**

Division of Applied Research and Technology, Centers for Disease Control and Prevention (CDC), National Institute for Occupational Safety and Health (NIOSH), Cincinnati, OH, USA

Abstract

Fiber dimension (especially length) and biopersistence are thought to be important variables in determining the pathogenicity of asbestos and other elongate mineral particles. In order to prepare samples of fibers for toxicology studies, it is necessary to develop and evaluate methods for separating fibers by length in the micrometer size range. In this study, we have filtered an aerosol of fibers through nylon screens to investigate whether such screens can efficiently remove the long fibers (L >20 μm, a typical macrophage size) from the aerosol stream. Such a sample, deficient in long fibers, could then be used as the control in a toxicology study to investigate the role of length. A well-dispersed aerosol of glass fibers (a surrogate for asbestos) was generated by vortex shaking a Japan Fibrous Material Research Association (JFMRA) glass fiber powder. Fibers were collected on a mixed cellulose ester (MCE) filter, imaged with phase contrast microscopy (PCM) and lengths were measured. Length distributions of the fibers that penetrated through various screens (10, 20 and 60 μm mesh sizes) were analyzed; additional study was made of fibers that penetrated through double screen and centrally blocked screen configurations. Single screens were not particularly efficient in removing the long fibers; however, the alternative configurations, especially the centrally blocked screen configuration, yielded samples substantially free of the long fibers.

Keywords

Aerosol; fiber length; glass fiber; nylon mesh screens; vortex shaker

Introduction

Length classification of airborne fibers is a fundamental technology important for toxicology studies of these materials. Many current fiber measurement techniques arose out of health concerns over asbestos exposure (Baron, 2001). Fiber toxicity appears to depend on fiber

Address for correspondence: Bon Ki Ku, Division of Applied Research and Technology, Centers for Disease Control and Prevention (CDC), National Institute for Occupational Safety and Health (NIOSH), 4676 Columbia Parkway, MS-R3, Cincinnati, OH 45226, USA. Tel: +1 513 841 4147. Fax: +1 513 841 4545. bku@cdc.gov.

Declaration of interest

The findings and conclusions in this report are those of the authors and do not necessarily represent the views of the National Institute for Occupational Safety and Health. Mention of product or company name does not constitute endorsement by the Centers for Disease Control and Prevention. None of the authors has a financial relationship with a commercial entity that has an interest in the subject of this manuscript. This study was funded by the NORA program at NIOSH.

concentration, dimensions (diameter and length) and durability in the lungs. Recently, the National Institute for Occupational Safety and Health (NIOSH) has published a Roadmap for research of asbestos fibers and other elongate mineral particles (EMPs), which attempts to focus research efforts towards a clearer understanding of the important determinants of toxicity for asbestos fibers and other EMPs (NIOSH, 2011). An underlying theme is that, in order to better understand the toxicity of fibers, it is necessary to develop methods for classifying fibers by length so as to enable toxicology studies to directly test length as a salient parameter.

In addition, during the past decade, other airborne fibrous particles, such as carbon nanotubes and carbon nanofibers, have elicited concern (Donaldson & Poland, 2009; Nel et al., 2006; NIOSH, 2007, 2009; Oberdörster et al., 2005), due to their asbestos-like morphology (Kisin et al., 2011; Poland et al., 2008). The thin fiber-like structure of these particles, and their presumed long biopersistence in the lungs, together suggest toxicity reminiscent of harmful asbestos fibers. These concerns have been corroborated by recent work (Shvedova et al., 2005).

Fiber length has long been suspected (Stanton et al., 1981) as being a crucial parameter which determines various toxicological responses (fibrosis, lung cancer and mesothelioma) to the presence of asbestos in the lung. Direct toxicological testing has been hampered by the inability to prepare significant quantities of length-classified asbestos samples. For a review of the potential pathogenicity of fiber length, see Dodson et al. (2003). Our recent work at NIOSH has focused on developing techniques to separate mineral fibers by length in order to prepare asbestos samples of well-defined length for subsequent toxicological study. This article reports on one aspect of that work with model glass fibers.

Various techniques are under investigation to prepare fibers longer or shorter than the size of a typical alveolar macrophage ($L_{\text{macro}\varphi}$~20 μm). NIOSH has extensively studied the use of the Baron dielectrophoresis-based fiber length classifier (FLC), which has been demonstrated to successfully separate fibers according to their lengths (Baron et al., 1994; Deye et al., 1999). Length separation has also been achieved (Chen et al., 1993) with electrically charged monodisperse-diameter carbon fibers. We have recently modified the aerosol generation parameters so as to enable the Baron instrument to process increased quantities of material. However, because of the input length distributions, and the inefficiencies inherent in aerosol separation (i.e. a long process time to obtain large quantity), it appears that this technique will only be useful to prepare short fiber material in sufficient quantities for toxicological study. It is thus important to develop alternative techniques for preparing large quantities of short fiber material.

In parallel with this study to improve the throughput of the Baron FLC, we have also studied the use of a cross-flow filtration technique of fiber suspensions in water (Bauer-McNett fiber classification), which has been successfully utilized in the paper industry to characterize pulp fiber length. We have extended the operation of the Bauer-McNett classifier from separation at the 10^{-3}–10^{-4}m scale (appropriate for pulp characterization) to the 10^{-5}m scale (appropriate for asbestos separation). It is anticipated that, in order to prepare samples

of length-separated asbestos fibers for toxicological study, the sample of the long fibers will be isolated with a liquid-based technique like the Bauer-McNett cross-flow separator.

Of equal importance to the preparation of samples of the presumably potent long fibers is the preparation of control samples, containing only shorter fibers (i.e. L<20 μm). The work reported here attempts to address this equally challenging problem. The screen separation technique of this study should be viewed as complementary to the Baron dielectrophoretic classification.

Researchers have used a variety of approaches to select fibers of well-defined lengths. Spurny et al. (1979) and Spurny (1980) used liquid sedimentation to separate asbestos and glass fibers by length, but relatively long times (e.g. 30 days) were required. Sedimentation has a weak (logarithmic) dependence on fiber length, so length separation using sedimentation is not sharp for a sample of fibers which are polydisperse in diameter, as well as length, because the settling depends linearly on the fiber diameter.

As mentioned above, Baron and colleagues (Baron et al., 1994; Deye et al., 1999) developed a dielectrophoresis-based FLC, which yields a relatively narrow length distribution of fibers (around a well-defined length with standard deviations ~20%). This classifier separates fibers by introducing them into a gradient electric field; the electric field polarizes the fibers and aligns them parallel to the field. The fibers migrate to regions of high electric field, with a drift velocity proportional to the square of the fiber length. The FLC was used to provide samples of glass fibers of several lengths for an *in vitro* toxicity study (Zeidler-Erdely et al., 2006); an important technological barrier for *in vivo* toxicology testing is the inability of the FLC to generate large (e.g. ~0.1 g) quantities of fibers in narrow length-classified size ranges (NIOSH, 2011).

In principle, using a screen as a filter should be a fast and easy-to-use method to classify airborne fibers in the length range of several micrometers to several hundred micrometers. The simplicity of the geometry permits easy scale-up so as to prepare a large amount of length-classified fibers for toxicology studies in a short time. The practicality of scaling up these research results into an engineering instrument, capable of producing a long-fiber depleted sample for use as a control in toxicology experiments, is discussed in Appendix 1. If one could harvest the screens, the method might also provide a way to recover the more potent medium and long fibers (captured on the screens due to interception) – however, we have only studied the short fibers that penetrate through the screen. Several studies have been conducted using a screen as a filter for length classification. Spurny et al. (1979) used sieving through vibrating screens of different mesh in an attempt to narrow down the fiber length distribution. Qualitative length separation was obtained only after several sievings; variation of the fiber length distribution, as a function of screen mesh size, was not explored. Myojo (1999) determined count median length of glass fiber aerosols using a Monte Carlo simulation and measurement of fiber penetration through wire mesh screens. However, the approach did not provide a high quality of length separation and was limited by particle loading on the screens (Myojo, 1999). Considering the promise of the technique, but the heretofore limited quantitative results, further investigation and improvement of the screen

technique was deemed a worthwhile approach to sample preparation for fiber toxicology studies.

The aim of this study was to explore the use of screens (housed in asbestos sampling cassettes) as a length separation method of airborne fibers and to evaluate how feasible the method would be to classify fibers in the micrometer size range. Well-dispersed glass fibers were generated by vortex shaking of glass fiber powder (Ku et al., 2006, 2012, 2013). The aerosol stream of fibers was “filtered” through screens of different screen mesh sizes (10, 20 and 60 μm), and the length distributions of the fibers in the penetrating aerosol stream were measured. Single screen configurations, as well as double screen, and the more complicated screen with central blockage, configurations were investigated. The uniformity of fiber loading on a filter downstream from the screen was also examined.

Materials

Glass fiber powder (GW1), supplied by the Japan Fibrous Material Research Association (JFMRA), was used as a surrogate for amphibole asbestos. In contrast, chrysotile asbestos is often longer, thinner, curved and more flexible, so rigid glass needles may be a less useful model material for the separation of chrysotile than amphibole asbestos. The glass fiber sample has a nominal geometric mean length (GML) L_{geom}~20.0 μm, with geometric standard deviation (GSD) ~2.58, and geometric mean diameter d_{geom}~0.88 μm, with GSD~3.10 (Kohyama et al., 1997).

Experimental methods

An aerosol of the glass fibers was prepared by a vortex shaking method (Ku et al., 2006, 2012, 2013). A schematic diagram of the experimental setup is shown in Figure 1. A batch of glass fiber powder (about 0.2 g) is placed at the bottom of a Pyrex test tube (OD 25 and 200mm in length, Thermo Fisher Scientific, Inc., Waltham, MA) and then is vigorously agitated by a vortex shaker (Vortex-Genie 2, Bohemia, NY). Air is introduced into the vortex shaker test tube, typically at a flow rate of 1.5 lpm; the out-flowing aerosol contains well-dispersed fibers. At this flow rate, the length distribution of the fibers in the aerosol is representative of the length distribution in the powder; however, at lower flow rates, the vortex shaker preferentially lofts only the smaller fibers (Ku et al., 2012, 2013). We have also observed a nontrivial long-time evolution of the aerodynamic diameter distribution (Ku et al., 2012, 2013), which may reflect length segregation within the agitated sample powder; while not completely understood, we are confident that the long time dependences seen in that study do not invalidate the results of the current measurements (taken over shorter times) reported here.

In order to measure the aerodynamic size distribution of the airborne glass fibers, the aerosol exiting from the vortex shaker tube is diverted into an aerodynamic particle sizer (APS model 3321, TSI Inc., St. Paul, MN); since the APS is run with a total flow rate of 5.0 lpm, the flow must be augmented by an additional stream of HEPA-filtered make-up air. It is known that the APS aerodynamic diameter is a weak function of particle shape factor (Brockmann & Rader, 1990; Cheng et al., 1990); we have not attempted to correct for this

and report (e.g. Figure 7) only the raw, as measured, APS aerodynamic diameter. In the collection mode, the APS is bypassed, and the airborne fibers are collected directly onto a mixed cellulose ester (MCE) filter (SKC Inc., Eighty Four, PA), mounted in a 25mm conductive cassette (#225-321A, SKC Inc.). The configuration of the sampling cassette, which contains both screen and filter, is shown in Figure 1 (bottom).

Nylon net screens (Millipore Corp., Billerica, MA), with different screen mesh sizes (60, 20 and 10 μm; models NY60, NY20 and NY10), were used to examine the effect of screen pore size on the length distribution of fibers penetrating through each screen. Nylon, instead of metal, screens were used in anticipation of future digestion or ashing of the screens so as to analyze the particulate matter collected on the screens – this analysis of intercepted fibers is not reported here. Also, the nylon screens have a wide range of available screen pore sizes (10–180 μm), which permits systematic investigation of the effect of screen pore size. At the end of this study, we also experimented with alternative screen configurations (e.g. double screens and a single screen with a blockage in its center), which will be described below. Scanning electron microscope (SEM) images of the three different screens used in this study are shown in Figure 2. All the screens have uniform nylon fiber diameters and reasonably uniform mesh pore sizes. From the SEM images, the apertures are roughly square, with measured sides a=10.6 ± 3.5 μm (10 μm screen), b=23±4 μm (20 μm screen), c=64±1 μm (60 μm screen); the 10 μm screen exhibits the largest deviation from square apertures. The two duplicates of the fiber samples were collected for length distribution measurement to ensure the effect of screen pore size on the length distribution of fibers penetrating through each screen.

The collected fibers were imaged by phase contrast microscopy (PCM), typically at 40× (although occasionally at 10×) magnification; length distributions were obtained from the statistics of the measured lengths. At the 1.5 lpm aerosol flow rates, the fibers were collected on the MCE filter for 5–20 s, depending on fiber concentrations. This sampling time was long enough to ensure a sufficient number of fibers for a statistically stable length distribution but short enough to prevent overloading of the filters.

Filter preparation and measurement of fiber length distributions

The as-received MCE filters are optically opaque. To use phase contract microscopy for length measurement, the fiber-loaded MCE filter needs to be clarified. Briefly, the fiber-loaded MCE filter was placed (fiber-side down) on a glass slide; the filter and slide were exposed to hot acetone vapor (about 1mL of liquid acetone is introduced into the top of an ETC Quick Fix acetone vaporizer, Environmental Monitoring Systems, Inc., Charleston, SC); as the acetone vapor permeates the MCE filter, it collapses and no longer scatters visible light, and the collected fibers may be imaged through an optical microscope.

Optical images were captured using a Nikon Labophot-2 microscope, with CCD camera (Moticam 2300, Motic Instruments, Inc., British Columbia, Canada). Motic Images Plus 2.0 ML was used to take images of the fiber sample. To systematically examine the loading of fibers on the filter, representative images were obtained every 2mm across the diameter of the entire filter. The first image was taken at the far left of the filter, where the first fibers are visible; the stage was then moved in 2mm intervals, and images were captured. This

procedure was repeated until no more fibers were visible (right-hand extreme image). At 40× magnification, this procedure usually yielded 10 fields per slide. The length of the fibers was then measured using the line tool from Motic Images Plus 2.0 ML (faint fibers were identified with the aid of the magnifier tool at 200% magnification); only fibers entirely contained within the field of view are included for length measurement. Length measurements were calibrated against a 150 μm dark round circle, captured at 40×. Typically, 300–800 fibers are imaged and measured; the length data is then statistically analyzed to obtain length distributions.

Results

Length distributions of glass fibers in the aerosol

Length distributions of the raw material (GW1) aerosolized by the vortex shaker were first investigated. Figure 3 shows representative images of the airborne glass fibers that were collected on the MCE filter. The images were taken from the left to the right across the filter along a diameter using a phase contract microscope. The number at the top left of each image indicates the distance from the far left of the filter, where the first fibers are detected. The aerosolized fibers are well dispersed by the vortex shaker generator, because the fibers collected on the filters show no evidence of agglomeration. We also have verified that the number density of fibers is rather uniform as the filter is sampled across its diameter; this is discussed below in more detail (discussion accompanying Figure 9).

Qualitatively, Figure 3 evinces a polydispersity in the length of these glass fibers. Quantitatively, the length distribution of the fibers is approximately lognormal (Figure 4), with a GML L_{geom} ~ 18.4 μm and geometric standard deviation, GSD~ 2.41. This is in reasonable agreement with the nominal GML L_{geom}~ 20.0 μm reported for the powder (Kohyama et al., 1997).

In the “Length distributions of glass fibers penetrated through a screen” section, length distributions are presented for different screen mesh sizes. In the “Loading of screen-penetrating fibers on the filter” section, we discuss the uniformity of fiber loading on the filters. In the “Length distributions using screens with different configurations” section, we discuss the effect of alternative screen configurations.

Length distributions of glass fibers penetrated through a screen

Figure 5 shows cumulative fractions of glass fibers penetrated through a screen as a function of fiber length for different screen sizes. For each screen, shown are two independent runs to illustrate our level of consistency – the fiber length distributions are all constructed from PCM images at 40× magnification. For comparison, the control for the case of no screen is also included, for the two independent runs. While not identical, the two distributions are very similar, with count median lengths L_{50}~ 18.4 μm (run 1) and L_{50}~ 18.3 μm (run 2). With no screen, the length distribution of the fibers is similar to that reported for the powder (Kohyama et al., 1997).

As soon as the screens are introduced, the median length (L_{50}) of the length distribution is substantially reduced, although this is not simply related to the aperture size: L_{50}~ 10 μm (60

μm screen), L_{50}~ 7.7 μm (20 μm screen) and L_{50}~ 6.2 μm (10 μm screen). For all screens, these median lengths are smaller than the nominal aperture size. For clarity, we have indicated, with colored vertical lines, the nominal aperture size L_{mesh}~ 10 μm (black), 20 μm (red) and 60 μm (blue). Again, the major effect with the introduction of any of the screens is to shift the entire distribution to shorter lengths.

The length distribution of the fibers that penetrate the screen remains lognormal; for the 10 μm screen (Figure 6), the GML L_{geom}~ 7.47 μm and geometric standard deviation, GSD~ 2.13. It is significant that the length distribution is narrower than the length distribution for the unfiltered aerosol of fibers. GMLs and GSDs for the three screens are summarized in Table 1.

Of relevance for toxicology samples is the potential use of screens to eliminate the population of long fibers. Taking $L_{macro\varphi}$ ~ 20 μm as a typical macrophage length, the original un-separated sample had 40% of the fibers longer than 20 μm; with screens, this can be reduced to ~ 20% (26% for the 60 μm screen, 15% for the 20 μm screen and 6% for the 10 μm screen). While promising as a method to prepare a control sample for toxicology experiments, where the control would be nominally devoid of the long fibers, a 20% contamination level is still too high for all but those markers which respond at least an order of magnitude more strongly to long than to short fibers. For a discussion of the consequences of contamination of the control by long fibers, see Appendix 2.

Figure 7 shows number concentration distributions as a function of aerodynamic diameter of the fibers for different mesh size screens, as measured by the APS situated downstream of the screen. In the absence of any screen, the aerosolized fibers exhibit a bimodal distribution, with a primary mode at the shorter aerodynamic diameter d_{aero}~ 1.5 μm and secondary mode at the larger aerodynamic diameter d_{aero}~ 7 μm. Introduction of any screen significantly reduces the secondary (large aerodynamic diameter) mode; in fact, the 10 μm screen significantly eliminates this mode. Insertion of the screens also systematically reduces the peak location of the primary mode: d_{aero}~ 1.2 μm for the 60 μm screen, d_{aero}~ 1.1 μm for the 20 μm screen and d_{aero}~ 1.0 μm for the 10 μm screen. Since the aerodynamic diameter depends linearly on the fiber physical diameter, but only logarithmically on the fiber physical length, these small shifts in measured aerodynamic diameter represent rather significant shifts in the physical length distributions of the aerosolized fibers that penetrate the screen. For additional discussion on the physical interpretation of the measured aerodynamic diameter, see Appendix 3.

Loading of screen-penetrating fibers on the filter

The loading of fibers on the filter was investigated by counting and measuring fibers across the diameter of the collection filter (sampled every 2 mm; Figure 9a, inset). Images of the fiber loading at four locations on the filter are shown (Figure 8) for each of the three screens. Spatial histograms of the number of fibers which penetrate through each screen are shown in Figure 9. With the exception of the experiment with the 10 μm screen, the fiber deposition is quite uniform across the filter; we suspect that a misalignment of the 10 μm screen might have introduced an asymmetric spurious flow which has skewed the fiber deposition in this experiment (low deposition at the left, high deposition at the right).

The average number of fibers collected per second per field of view (200 μm × 250 μm at 40×) is 9.6 for the 60 μm screen, 9.2 for the 20 μm screen and 5.3 for the 10 μm screen; this should be compared with 11.1 for the case with no screen present. This reduction in fiber deposition is, of course, related (albeit not simply) to the finite porosity of the screens. The total flux of fibers is only slightly reduced by the presence of the screens and depends only weakly on the screen porosity.

Length distributions using screens with different configurations

We also investigated two additional screen configurations. The first "double screen" configuration consists of two screens positioned back to back (at random azimuthal alignment). The second "centrally blocked" configuration introduces a blocking disk at the center of the screen (Figure 10 inset). Figure 10 shows cumulative fractions of fibers collected under these three conditions: single screen, double screen and centrally blocked screen for: (a) 60 μm, (b) 20 μm and (c) 10 μm screens. Using either the double screen or centrally blocked screen configuration tends to sharpen the length distribution of the penetrating fibers (i.e. it reduces both the long and short fiber "tails"); this effect is more pronounced for the smaller aperture screens. There appears to be minimal effect on the midpoint of the length distributions for these alternative configurations (double screen or centrally blocked screen), as compared with the corresponding single screen. The GMLs and geometric standard deviations of the length distributions for these alternative configurations are also given in Table 1. Again, with the aim of using the screens to filter out long fibers, so as to prepare a control sample for toxicology studies, we see that the fraction of fibers longer than $L_{\text{macro}\varphi} \sim 20$ μm can be significantly reduced by using either the double screen configuration (25, 2 and 3% for 60, 20 and 10 μm screens, respectively), or the centrally blocked screen configuration (18, 6 and 6% for 60, 20 and 10 μm screens, respectively). Levels of contamination of 5% now make possible the use of this technique to prepare a short fiber control (Appendix 2).

Discussion

Interposing a screen into an aerosol fiber stream shifts the entire downstream fiber length distribution to smaller lengths, compared to the fiber length distribution of the upstream aerosol stream. The sharpness of the fiber length distribution is degraded using a single open screen (60 and 20 μm) but not by the finer (10 μm) screen. The alternative configurations (double screens and the centrally blocked screen) do appear to sharpen the fiber length distributions, especially with the finer (20 and 10 μm) screens. In this section we discuss potential mechanisms that could affect the fiber length distribution.

The flows throughout this experiment are laminar. At volumetric flow rate Q=1.5 lpm, in a 25mm sampling cassette (with effective diameter d~ 22 mm), the superficial flow velocity is U~ 6.6 cm/s, corresponding to Reynolds number, $\text{Re}=Ud/\nu \sim 100$, where $\nu \sim 0.15$ cm^2/s is the kinematic viscosity for air. The flow in the cassette is not fully developed Poiseuille flow, due to the sudden radial expansion from the small cassette inlet (d=4 mm) to the body of the cassette (d=25 mm). Orientation of fibers near the walls of such sudden expansion flows have been reported (Yasuda et al., 2005), but in the dilute regime (appropriate for an

aerosol), this orientation is merely the result of high shear near the wall, as would be the case of Poiseuille flow, and the random orientation near the center reflects the relative lack of shear for Poiseuille flow near the axis. It would thus appear that a quasi-Poiseuille description for the macroscopic flow in the cassette is appropriate, and that the complication associated with the sudden expansion of the flow from the inlet can be ignored.

The finite porosity of the screens, defined as a ratio of open area to total area of a screen, $a \sim 0.41$ (60 μm screen), $a \sim 0.14$ (20 μm screen) and $a \sim 0.04$ (10 μm screen), due to the obstruction of the nylon wires, enhances the superficial velocities that transit the screens: $U \sim 16$ cm/s (60 μm screen), $U \sim 47$ cm/s (20 μm screen) and $U \sim 165$ cm/s (10 μm screen). However, because the aperture size is also reduced, the Reynolds numbers remain small, Re~ 0.6 (60 and 20 μm screens), Re~ 1 (10 μm screen).

We believe that impaction plays a minor role in these screen experiments. The Stokes number is given by (Hinds, 1999)

$$\mathrm{Stk}=\frac{\rho_\mathrm{p}}{\rho_\mathrm{g}}\frac{d_\mathrm{p}^2 U}{18D}\sim 0.02$$

where ρ_p and ρ_g are the particle and gas densities, d_p the particle aerodynamic diameter (~ 1 μm), D the screen wire diameter (~ 30 μm) and U the velocity near the screen (~ 7 cm/s). Since Stk $\ll 1$, the fibers follow the streamlines.

While still laminar, there is high shear associated with the constriction of the quasi-Poiseuille flow (within the body of the cassette) into the “jets” through the apertures. For small fibers, where we may neglect the effect of inertia, this high shear exerts a torque on each fiber, which results in Jeffery rotation of the fiber about its centroid (Jeffery, 1922). This tumbling of the fiber in the neighborhood of the screen permits the screen to intercept a fraction of the impinging fibers. This description is appropriate for those fibers small enough to be carried along with the streamlines of the flow. The very long fibers have enough inertia to potentially cross streamlines and impact onto the screen. Despite Stk $\ll 0.1$, the effects of inertia seems to dominate for the case of the centrally blocked screens (discussed below) and are thus probably equally important in the simple screen configuration. Diffusion is negligible for fibers at the micrometer length scale.

Despite the overall reduction in the fiber length distribution, due to the interposition of the screens, the filtering by the screens is a relatively inefficient process. The percentage of fibers longer than the aperture size is still appreciable: probability (L>60 μm)=0.03 for the 60 μm screen, probability (L>20 μm)=0.14 for the 20 μm screen and probability (L>10 μm)=0.28 for the 10 μm screen; i.e. a significant fraction of fibers longer than the aperture size penetrate the screen. Furthermore, while the overall length distribution is shifted to shorter fiber lengths, the GSD is essentially unchanged from the incident aerosol (Table 1). We believe that the depletion of the long fibers from the air stream is governed by fiber alignment parallel to the screens (see below). Any modification of the flow which enhances this alignment is likely to improve the depletion of the longer fibers.

The case for the double screen configuration is qualitatively similar; the porosities are not known but are presumably reduced. The flows are locally more complicated, again with high shear associated with the constriction of the overall flow through the apertures. It is surprising, however, that this configuration results in a fiber length distribution sharper than that which is obtained from the single screen configuration: GSD_{double}~ 2.43<GSD_{single}~ 2.86 for the 60 μm screen; GSD_{double}~ 2.00<GSD_{single}~ 2.89 for the 20 μm screen; GSD_{double}~ 1.78<GSD_{single}~ 2.22 for the 10 μm screen.

The case for the centrally blocked screen configuration is qualitatively different. The quasi-Poiseuille flow (within the body of the cassette) encounters the central disk obstruction and is diverted radially outward where it penetrates an annular screen. The small fibers (zero inertia) might be expected to follow a Jeffery model. There is macroscopic shear associated with this flow diversion; superimposed on this macroscopic shear is the shear arising from the constriction into the "jets" through the apertures in the unobstructed screen. Again, this shear gives rise to additional Jeffery tumbling of the fibers, thereby increasing the efficiency of the screens in removing the longer fibers. For the larger fibers, even though Stk $\ll$ 1, inertial effects probably need to be considered. For the centrally blocked configuration, the flow is diverted radially outward, and the fibers are aligned with the flow. When the flow redirects around the blockage to go through the screen, fibers that were parallel to the screen, due to their inertia cannot respond to the change in flow direction, and are thus intercepted by the screen. The more aligned the fibers are parallel to the plane of the screen, the greater their potential for interception by the screen. It would seem that this centrally blocked screen configuration achieves this alignment to some degree. This is precisely the geometry of flow against an impactor; imaging photomicrographs of deposits of long chain aggregates, Kasper & Shaw (1983) have shown that the long chain aggregates were aligned parallel to the radial flow field. This stagnation flow was simulated by Broday et al. (1997), who found that, irrespective of the initial fiber orientation, the fibers align parallel to the collector surface.

It is remarkable that this configuration significantly sharpens the fiber length distribution: GSD~ 2.26 (60 μm centrally blocked screen), GSD~ 1.94 (20 μm centrally blocked screen) and GSD~ 1.79 (10 μm centrally blocked screen). With this configuration, the fraction of fibers longer than a typical macrophage ($L_{macro\varphi}$ ~ 20 μm) is 0.18 (60 μm centrally blocked screen), 0.06 (20 μm centrally blocked screen) and 0.06 (10 μm centrally blocked screen). This latter value would be quite acceptable to be used for a short fiber control in a toxicology experiment (Appendix 2). Nonetheless, even this length separation resolution of fibers by centrally blocked screens is not higher than the length resolution obtained by the Baron FLC (Baron et al., 1994; Deye et al., 1999).

As a final remark, over time, fibers will accumulate on the screens, which will then require cleaning and/or replacement. These deposits will become important if extensive filtering is to be used to collect a sufficient fiber sample for toxicological testing. The effect of fiber loading on length separation has not been investigated in this study and needs to be investigated further.

Conclusions

In this study, filtration of airborne fibers by screens was investigated as a means to prepare toxicology samples free of long fibers. Three different screen mesh sizes were used to classify glass fibers, and their 50% cut-off length, GML, and geometric standard deviation were obtained, based on a phase contrast microscopy. The fibers were aerosolized by a simple vortex shaker.

1. With no screen, the length distribution of the aerosolized fibers (L_{geom}~ 18.4 μm) is similar to that of the powder (L_{geom}~ 20 μm).
2. With the interposition of any screen into the aerosol flow, the entire length distribution shifts to shorter lengths: L_{geom}~ 12.8 μm (60 μm screen), L_{geom}~ 9.2 μm (20 μm screen), L_{geom}~ 7.3 μm (10 μm screen). However, the width of the distribution, GSD~ 2.86 (60 μm screen) and GSD~ 2.88 (20 μm screen), is degraded from that of the incident aerosol, GSD~ 2.36, although the aerosol that penetrates the finer screen (10 μm) has a comparable GSD~ 2.22.
3. The aerodynamic diameter of the aerosolized fibers evinces a bimodal distribution (modes at d_{aero}~ 1.5 μm and 7 μm). The interposition of the screens significantly reduces the weight in the higher, secondary mode, as well as slightly reducing the location of the lower, primary mode.
4. Using double screens slightly improves the removal of the longer fibers. For the 60 μm screen, L_{geom}~ 12.0 μm (double) ~ L_{geom}~ 12.8 μm (single) with GSD_{double} ~ 2.43<GSD_{single}~ 2.86; similarly, for the 20 μm screen, L_{geom}~ 7.2 μm (double) ~ L_{geom}~ 9.3 μm (single) with GSD_{double}~ 2.00<GSD_{single}~ 2.88; finally, for the 10 μm screen, L_{geom}~ 5.2 μm (double) ~ L_{geom}~ 7.3 μm (single) with GSD_{double}~ 1.78<GSD_{single}~ 2.22
5. Using centrally blocked screens significantly improves the removal of longer fibers. For the 60 μm screen, L_{geom}~ 10.8 μm (blocked) ~ L_{geom}~ 12.8 μm (unblocked) with $GSD_{blocked}$~ 2.26<$GSD_{unblocked}$~ 2.86; similarly, for the 20 μm screen, L_{geom}~ 7.2 μm (blocked) ~ L_{geom}~ 9.3 μm (unblocked) with $GSD_{blocked}$ ~ 1.94<$GSD_{unblocked}$~ 2.8; finally, for the 10 μm screen, L_{geom}~ 4.8 μm (blocked) ~ L_{geom}~ 7.3 μm (unblocked) with $GSD_{blocked}$~ 1.79<$GSD_{unblocked}$~ 2.22.
6. Using centrally blocked screens yielded samples relatively free from long fibers, $L>L_{macro\varphi}$ ~ 20 μm. For the centrally blocked 60 μm screen, only 18% of the fibers have lengths which exceed $L_{macro\varphi}$ ~ 20 μm; for the centrally blocked 20 μm and 10 μm screens, only 6% of the fibers have lengths which exceed $L_{macro\varphi}$ ~ 20 μm. This latter would be quite acceptable to use as a control sample for a toxicology test of length. This stripping of the long fibers out of the aerosol is significant; it should be compared with the incident aerosol, where 40–50% of the fibers have lengths which exceed $L_{macro\varphi}$ ~ 20 μm.
7. This study has demonstrated the selectivity of a variety of screen configurations to deplete long fibers from an aerosol stream. While still in the research stage, it is anticipated that this technology may be scaled up to a throughput, capable of

preparing $M \sim 0.1$ g of short fibers. The practicality of using this technology is discussed in Appendix 1.

Acknowledgments

The authors thank Mariko Ono-Ogasawara (Japan National Institute of Occupational Safety and Health, and Japan Fibrous Material Research Association, JFMRA) for the samples of the GW1 glass fibers used in this study. We thank Joe Fernback (NIOSH), for SEM images, and Elizabeth Ashley (University of Cincinnati), for assisting in the analysis of PCM images of the fibers. We thank Pramod Kulkarni and Chaolong Qi for helpful discussions. We thank the referees of the initial version of our manuscript for prompting the discussion contained in the Appendices. We thank the referee of the revised manuscript for the fiber inertia argument ("Discussion" section), rationalizing the efficacy of the centrally blocked screen configuration.

References

Baron PA, Deye GJ, Fernback J. Length separation of fibers. Aerosol Sci Technol. 1994; 21:179–92.

Baron PA. Measurement of airborne fibers: a review. Ind Health. 2001; 39:39–50. [PubMed: 11341557]

Blake T, Castranova V, Schwegler-Berry D, et al. Effect of fiber length on glass microfiber cytotoxicity. J Toxicol Environ Health A. 1998; 54:243–59. [PubMed: 9638898]

Brockmann JE, Rader DJ. APS response to nonspherical particles and experimental-determination of dynamic shape factor. Aerosol Sci Technol. 1990; 13:162–72.

Broday D, Fichman M, Shapiro M, Gutfinger C. Motion of diffusionless particles in vertical stagnation flows. II. Deposition efficiency of elongated particles. J Aerosol Sci. 1997; 28:35–52.

Chen BT, Yeh HC, Hobbs CH. Size classification of carbon-fiber aerosols. Aerosol Sci Technol. 1993; 19:109–20.

Cheng YS, Chen BT, Yeh HC. Behavior of isometric nonspherical aerosol-particles in the aerodynamic particle sizer. J Aerosol Sci. 1990; 21:701–10.

Cox RG. The motion of long slender bodies in a viscous fluid I: General theory. J Fluid Mech. 1970; 44:791–810.

Deye GJ, Gao P, Baron PA, Fernback J. Performance evaluation of a fiber length classifier. Aerosol Sci Technol. 1999; 30:420–37.

Dodson RF, Atkinson MA, Levin JL. Asbestos fiber length as related to potential pathogenicity: a critical review. Am J Ind Med. 2003; 44:291–7. [PubMed: 12929149]

Donaldson K, Poland CA. Nanotoxicology: new insights into nanotubes. Nat Nanotechnol. 2009; 4:708–10. [PubMed: 19893519]

Fuchs, NA. The mechanics of aerosols. Oxford: Pergamon Press; 1964. p. 37-46.

Gans R. Sitzunder (Math. – Phys). Klasse Akad Wiss. 1911; 41:191–203.

Gonda I, Abd El Khalik AF. On the calculation of aerodynamic diameters of fibers. Aerosol Sci Technol. 1985; 4:233–8.

Griffiths WD, Vaughan NP. The aerodynamic behavior of cylindrical and spheroidal particles when settling under gravity. J Aerosol Sci. 1986; 17:53–65.

Hinds, WC. Aerosol technology: properties, behavior, and measurement of airborne particles. New York, USA: John Wiley & Sons; 1999.

Jeffery GB. The motion of ellipsoidal particles immersed in a viscous fluid. Proc R Soc Lond. 1922; 102:161–79.

Kasper G, Shaw DT. Comparative size distribution measurements on chain aggregates. Aerosol Sci Technol. 1983; 2:369–81.

Kisin ER, Murray AR, Sargent L, et al. Genotoxicity of carbon nanofibers: are they potentially more or less dangerous than carbon nanotubes or asbestos? Toxicol Appl Pharmacol. 2011; 252:1–10. [PubMed: 21310169]

Kohyama N, Tanaka I, Tomita M, et al. Preparation and characteristics of standard reference samples of fibrous minerals for biological experiments. Ind Health. 1997; 35:415–32. [PubMed: 9248227]

Ku, BK.; Deye, G.; Turkevich, LA. Characterization of a vortex shaking method for producing airborne glass fibers for toxicology studies. Nanotechnology 2012, Volume 3: Bio Sensors, instruments, medical, environment and energy. Chapter 5: Environment, health & safety. Technical Proceedings of the 2012 NSTI (NSTI-Nano Science and Technology Institute, Taylor & Francis: Boca Raton, FL, 2013), Nanotechnology Conference and Expo; June 18–21, 2012; Santa Clara, California. 2012. p. 358

Ku BK, Deye G, Turkevich LA. Characterization of a vortex shaking method for aerosolizing fibers. Aerosol Sci Technol. 2013; 12:1293–301.

Ku BK, Emery MS, Maynard AD, et al. In situ structure characterization of airborne carbon nanofibres by a tandem mobility-mass analysis. Nanotechnology. 2006; 17:3613–21. [PubMed: 19661613]

Morigi MP, Giacomelli GM, Prodi V. Mineral fibre sampling and size selection. Ann Occup Hyg. 1999; 43:117–24. [PubMed: 10206040]

Myojo T. A simple method to determine the length distribution of fibrous aerosols. Aerosol Sci Technol. 1999; 30:30–9.

Nel A, Xia T, Mädler L, Li N. Toxic potential of materials at the nanolevel. Science. 2006; 311:622–7. [PubMed: 16456071]

NIOSH. [Last accessed: Mar 2011] Progress toward safe nanotechnology in the workplace: a report from the NIOSH Nanotechnology Research Center. 2007. [DHHS (NIOSH) Publication No. 2007-123]. Available from: http://www.cdc.gov/niosh/docs/2007-123/pdfs/2007-123.pdf

NIOSH. [Last accessed: Mar 2011] Approaches to safe nanotechnology: managing the health and safety concerns associated with engineered nanomaterials. 2009. [DHHS (NIOSH) Publication No. 2009-125]. Available from: http://www.cdc.gov/niosh/docs/2009-125/pdfs/2009-125.pdf

NIOSH. [Last accessed: Jan 2012] Asbestos fibers and other elongate mineral particles: state of the science and roadmap for research. 2011. [DHHS (NIOSH) Publication No. 2011-159]. Available from: http://www.cdc.gov/niosh/docs/2011-159/pdfs/2011-159.pdf

Oberdörster G, Maynard A, Donaldson K, et al. Principles for characterizing the potential human health effects from exposure to nanomaterials: elements of a screening strategy. Part Fiber Toxicol. 2005; 2:8. 1–35.

Oseen CW. Uber den Wiederstand gegen die gleichmassige Translation eines. Ellipsoides in einer reibenden Flussigkeit. Arch Math Phys. 1915; 24:108–14.

Oseen, CW. Mathematik und ihre Anwendungen in Monographien und Lehrbüchern. In: Hilb, E., editor. Neuere Methoden und Ergebnisse in der Hydrodynamik. Vol. 1. Leipzig: Akademischer Verlagsgesellschaft; 1927.

Poland CA, Duffin R, Kinloch I, et al. Carbon nanotubes introduced into the abdominal cavity of mice show asbestos-like pathogenicity in a pilot study. Nat Nanotechnol. 2008; 3:423–8. [PubMed: 18654567]

Prodi V, Dezaiacomo T, Hochrainer D, Spurny K. Fiber collection and measurement with the inertial spectrometer. J Aerosol Sci. 1982; 13:49–58.

Shvedova AA, Kisin ER, Mercer R, et al. Unusual inflammatory and fibrogenic pulmonary responses to single-walled carbon nanotubes in mice. Am J Physiol Lung Cell Mol Physiol. 2005; 289:L698–708. [PubMed: 15951334]

Spurny KR, Stober W, Opiela H, Weiss G. Size-selective preparation of inorganic fibers for biological experiments. Am Ind Hyg Assoc J. 1979; 40:20–38. [PubMed: 484448]

Spurny, KR. Fiber generation and length classification. In: Willeke, K., editor. Generation of aerosols and facilities for exposure experiments. Ann Arbor, MI: Ann Arbor Sciences Publishers; 1980. p. 257-98.

Stanton MF, Layard M, Tegeris A, et al. Relation of particle dimension to carcinogenicity in amphibole asbestoses and other fibrous minerals. J Natl Cancer Inst. 1981; 67:965–75. [PubMed: 6946253]

Yasuda K, Henmi S, Mori N. Effects of abrupt expansion geometries on flow-induced fiber orientation and concentration distributions in slit channel flows of fiber suspensions. Polym Compos. 2005; 26:660–70.

Zeidler-Erdely PC, Calhoun WJ, Ameredes BT, et al. In vitro cytotoxicity of Manville Code 100 glass fibers: effect of fiber length on human alveolar macrophages. Part Fibre Toxicol. 2006; 3:5. 1–7. [PubMed: 16569233]

Appendix 1

Practicality of size separation of fibers by this method

It is useful to address the practicality of the screen separation method. These include issues such as:

1. The length of time required to separate a given quantity of fiber.
2. The feasibility to size separate fibers in sufficient quantity (in a reasonable time) to generate the amounts of test material required for an inhalation study.
3. The efficiency of the process: the amount of raw material required to generate a sufficient quantity of size separated material.

The technique which is described in this study is still in the research mode, where we are evaluating whether, in principle, screens can be used for length separation of fibers. We have presented evidence that the technique has reasonable selectivity. We do not claim to already have an operational instrument that can prepare M~ 0.1 g of sample (the quantity required for an inhalation toxicology experiment).

In order to implement the technique so as to actually prepare samples for toxicology testing, a moderate amount of scale-up is required. The following “back-of-the-envelope” engineering estimate indicates that this is not unrealistic.

We have two measured estimates of the fiber flux (e.g. using the 20 micron screen):

a. Downstream of the 20 micron screen, the APS measures a fiber concentration of about 200/cm^3 (the concentration in Figure 7). Since the APS samples at Q=5 L/min, this corresponds to a number flux of dN/dt~ 2 ×10^4 fibers/s.

b. From the microscopy, with a 20 micron screen, we typically see ~ 150 fibers/field (Figure 10). There are ~ 5×10^3 fields/filter. Since we have collected for Δt~ 20 s, this gives a number flux of dN/dt~ 4×10^4 fibers/s.

Thus, with the 20 micron screen, a reasonable estimate of the fiber number flux is dN/dt~ 3 (±1)×10^4 fibers/s.

Since a typical fiber (d~ 1 micron, L~ 10 micron) has mass M~ 2×10^{-11} g, the above number flux corresponds to a mass flux of dM/dt~ 6×10^{-7} g/s. In order to collect 10^{-1} g (the typical quantity required for a toxicology experiment) would thus require Δt~45 h of collection.

We estimate needing to use the entire 0.2 g charge of fibers in the vortex shaker for each hour of collection. Thus, collection of M~0.1 g of separated material will require ~9g of raw material.

We have shown (Ku et al., 2012, 2013) that the vortex shaker (our aerosol generator) is not stable over such a long time of operation. We thus expect that it will be necessary to

repeatedly replenish and restart the vortex shaker. Hence, a collection time of Δt~45 h would probably translate into a real operating time of Δt~150 h.

As the device is relatively simple, the anticipated mode of operation would be to configure several of these devices in parallel. This would proportionately reduce the total time needed for collection of the desired sample.

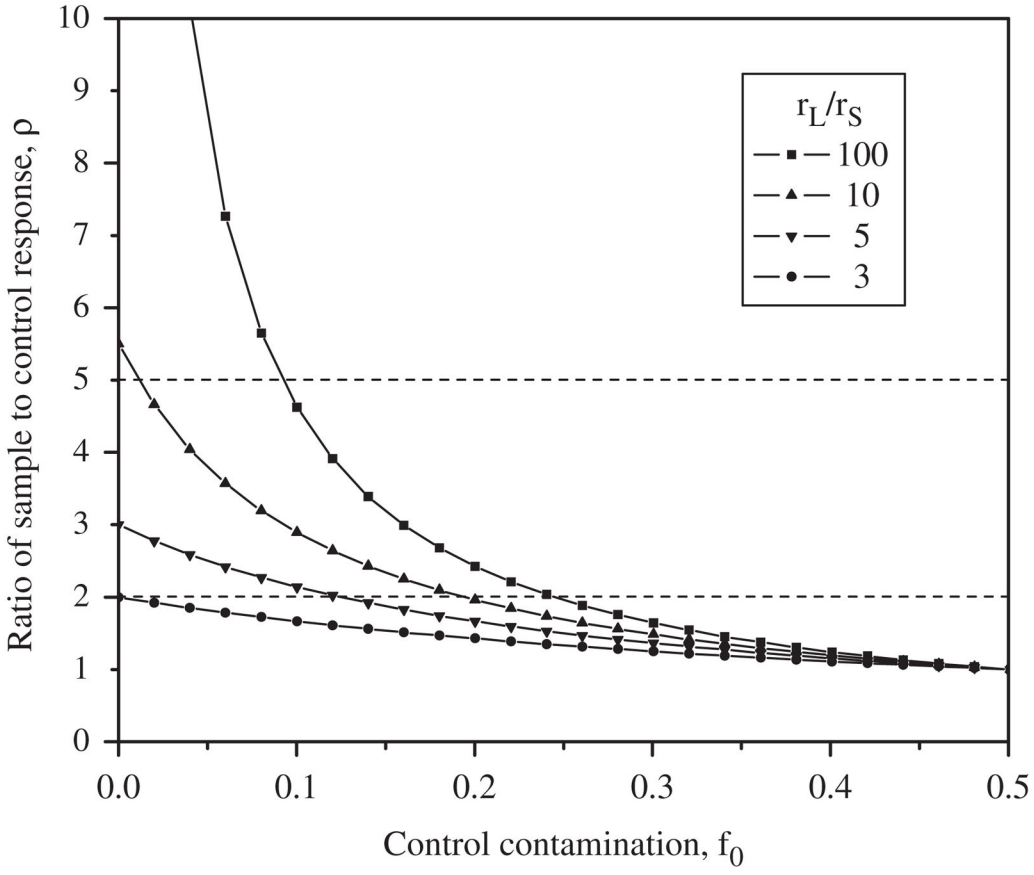

Figure A1.
Ratio of sample to control response, $\rho = R_L/R_S$, as a function of control contamination, f_0, for various marker response ratios, r_L/r_S. The simple two state response model is described in Appendix 2.

Appendix 2

Estimate of the consequences of contamination

Since the initial and separated fiber length distributions are continuous, it is important to estimate the extent of separation required in order to construct a meaningful toxicology experiment. A meaningful toxicology experiment should be able to establish whether there is a significant difference in response between long and short fibers of the given bio-persistent mineral (e.g. asbestos).

We assume that the response per fiber, r, of some marker is different for long and short fibers. A simple bimodal model is that the response per fiber differs above/below a length cutoff, L_c, namely that $r=r_S$ ($L<L_c$) and $r=r_L$ ($L>L_c$), where we anticipate that $r_L \gg r_S$.

For the "sample", with a population of fibers of different lengths, let f denote the fraction of fibers longer than the cutoff, L_c. Assuming a linear dose-response, the measured response to this population of fibers is $R_L=N\,[(1-f)r_S+f\,r_L]$, where N is the number of fibers in the dose.

Using some separation technique (e.g. a screen configuration), we prepare a "short fiber control", with a smaller fraction, f_0, of the long fibers ($L>L_c$); f_0 thus represents the level of long fiber contamination of the short fiber control. The measured response to the control is $R_S = N\,[(1-f_0)\,r_S+f_0\,r_L]$.

Thus, if we compare experimental responses of sample and control at comparable number doses of fibers, the toxicology experiment will measure the ratio

$$\rho=R_L/R_S=[1+(r_L/r_S-1)f]/[1+(r_L/r_S-1)f_0].$$

Clearly, if we had perfect separation, $f=1$ (only long fibers in the "sample"), $f_0=0$ (only short fibers in the "control"), then $\rho=r_L/r_S$. We want to assess how detrimental is the effect of a contaminated control ($f_0>0$).

Consider the "worst case" scenario where no effort has been made to enrich the "sample" with long fibers, i.e. where the long fiber sample possesses an unseparated population (for our glass fiber samples, f~0.5 for L_c~20 μm). Figure A1 plots the measured response ratio, ρ, as a function of contamination, f_0, of the control for several possible ratios, $r=r_L/r_S$, of fiber response. At low contamination (f_0~0), the measured response ratio reflects the ratio of responses to long and short fibers. As the contamination increases, the ratio of sample to control responses decreases, becoming indistinguishable ($\rho\rightarrow1$) when the control contamination approaches the fraction of long fibers in the sample ($f_0\rightarrow f$).

We now assess the level of contamination that can be tolerated. This depends on both the ratio, r_L/r_S, of responses to the long and short fibers, and also on the discrimination level, ρ_{min}, of the toxicology experiment. It would appear that $r_L/r_S \sim 10^2$ for both markers in the earlier NIOSH *in vitro* study (Blake et al., 1998) – suppression of zymosan stimulated alveolar macrophage chemiluminescence, and alveolar macrophage lactate dehydrogenase release – but not all markers can be expected to be this lopsided in their response. For example, if the toxicology experiment can determine only a fivefold difference between sample and control ($\rho_{min}=5$), then, at $r_L/r_S=100$, we can tolerate a contamination level of $f_0=0.09$ in the control, but at $r_L/r_S=10$, only a contamination level of $f_0=0.01$, and for $r_L/r_S<5$, it will not be possible to discriminate between the sample and the control. However, if the toxicology experiment has better resolution and can detect a twofold difference between sample and control ($\rho_{min}=2$), then at $r_L/r_S=100$, we can tolerate a higher contamination level of $f_0=0.25$ in the control, at $r_L/r_S=10$, f_0~0.20, but at $r_L/r_S=3$, only f_0~0.05. Thus, the larger the difference in response to long and short fibers (i.e. the larger the ratio r_L/r_S), the more

forgiving the experiment is to contamination, f_0, of the control; similarly, the better the experiment is able to measure the overall response, and hence to distinguish a different response from the sample than from the control (i.e. the lower the threshold, ρ_{min}), again, the more forgiving is the experiment to contamination, f_0, of the control.

Figure A2.
Cumulative fractions of fibers penetrating through 60 μm screen: length (solid square) as measured by SEM and (open square) as measured by PCM; diameter (solid circle) as measured by SEM; aerodynamic diameter, d_{ae} (open triangle), as measured by APS, and as calculated, d_{Cox} (solid line) using the Cox expressions or d_{sph} (dashed line) using the prolate spheroid expressions.

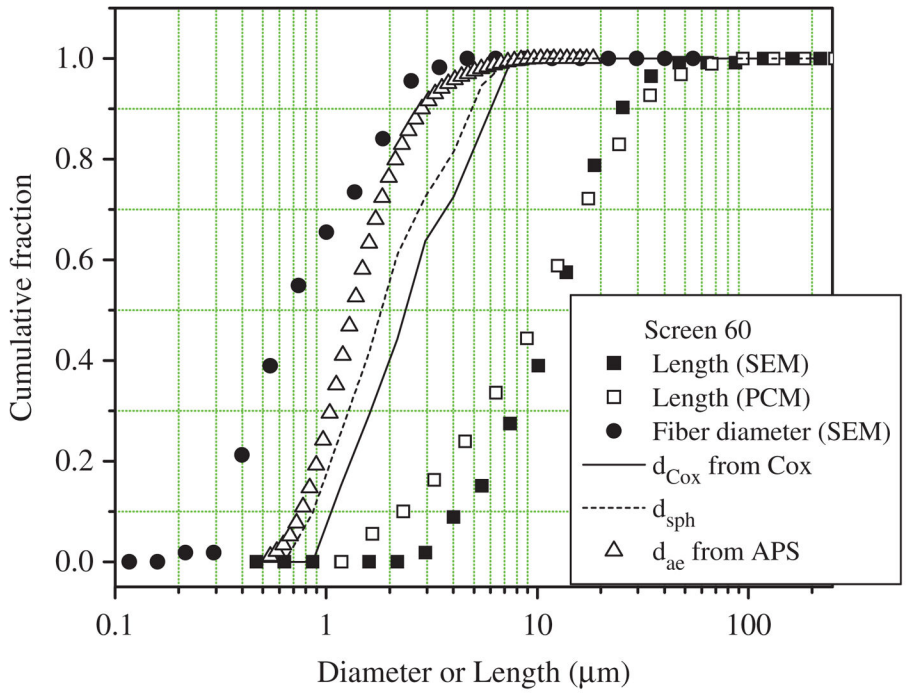

Appendix 3

Theoretical understanding of the measured aerodynamic diameter

While it is possible to compare the effect of interposing screens on the distribution of the aerodynamic diameter of fibers in the aerosol stream, the magnitude of the measured aerodynamic diameter is not theoretically understood. Shown (Figure A2) are the SEM measured fiber lengths (solid squares) and diameters (solid circles) for the aerosol penetrating the 60 μm screen. We have used this aerosol stream for the present discussion because the measured (APS) aerodynamic diameter is approximately single mode (Figure 7). As an aside, the fiber lengths, as measured by PCM, are also shown (open squares); the PCM and SEM lengths agree for L>10 μm, but PCM systematically overcounts the small fibers (L<10 μm), possibly due to misidentification of filter substrate defects (filter roughness) as fibers. Also shown is the aerodynamic diameter, d_{ae}, that is measured by the

APS for this aerosol stream (open triangles); the aerodynamic diameter clearly interpolates between the physical fiber length, *L*, and the physical fiber diameter, *d*, being closer to the latter.

In principle, the aerodynamic diameter should be calculable using the measured physical dimensions and known density. Cox (1970) has derived expressions (using the technique of matched asymptotic expressions), correct only to lowest order in the logarithm of the aspect ratio, for right cylinders in motion parallel and perpendicular to the long axis:

$$d_{\parallel}=d\{9\rho_f/4\rho_0[\ln(2\beta)-0.807]\}^{1/2}$$
$$d_{\perp}=d\{9\rho_f/8\rho_0[\ln(2\beta)+0.193]\}^{1/2}$$

where the aspect ratio $\beta=L/d$, and the fiber and unit densities are respectively ρ_f and ρ_0. For a random orientation,

$$d_{\mathrm{Cox}}=(d_{\parallel}+2d_{\perp})/3.$$

A similar expression has been derived (Fuchs, 1964; Gans, 1911; Oseen, 1915, 1927) for prolate spheroids, again for the two orientations of the long axis:

$$d_{\mathrm{sph}}=(\rho_f/\rho_0)^{1/2}(\beta/\chi)^{1/2}2a$$

where *a* is the semi-minor axis of the spheroid, ξ is the shape factor and where

$$\chi_{\perp}=\tfrac{8}{3}(\beta^2-1)\left\{\frac{2\beta^2-3}{\sqrt{\beta^2-1}}\ln(\beta+\beta^2-1)+\beta\right\}^{-1}$$
$$\chi_{\parallel}=\tfrac{4}{3}(\beta^2-1)\left\{\frac{2\beta^2-1}{\sqrt{\beta^2-1}}\ln(\beta+\beta^2-1)-\beta\right\}^{-1}$$

While exact (in the same sense that the Stokes drag formula for spheres is “exact”), it leaves open which parameters for the spheroid to use to model the fiber (asymptotically, the Oseen and Cox expressions do not agree and require adjustment of both semi-major and semi-minor axes). Attempts to patch up the Oseen expression by converting for differences in volume or mass (Gonda & Abd El Khalik, 1985) are ad hoc and unconvincing.

We have taken these theoretical expressions at face value and have calculated aerodynamic diameters, using the SEM measured lengths and diameters (solid line d_{Cox}, dashed line d_{sph} in Figure A2).

The two theoretical expressions overestimate the APS measured aerodynamic diameter by a factor of ~1.5. We conclude that a quantitative prediction of our measured aerodynamic diameter for fibers, on the basis of their measured physical dimensions, has still not been achieved. This lack of agreement between theoretically estimated and experimentally

measured aerodynamic diameters has been encountered by previous workers (Griffiths & Vaughan, 1986; Morigi et al., 1999; Prodi et al., 1982). Despite this lack of quantitative understanding, the measured aerodynamic diameter is still a useful diagnostic to compare (Figure 7) the fiber characteristics of different aerosol streams (e.g. as they are modified by the interposition of screens).

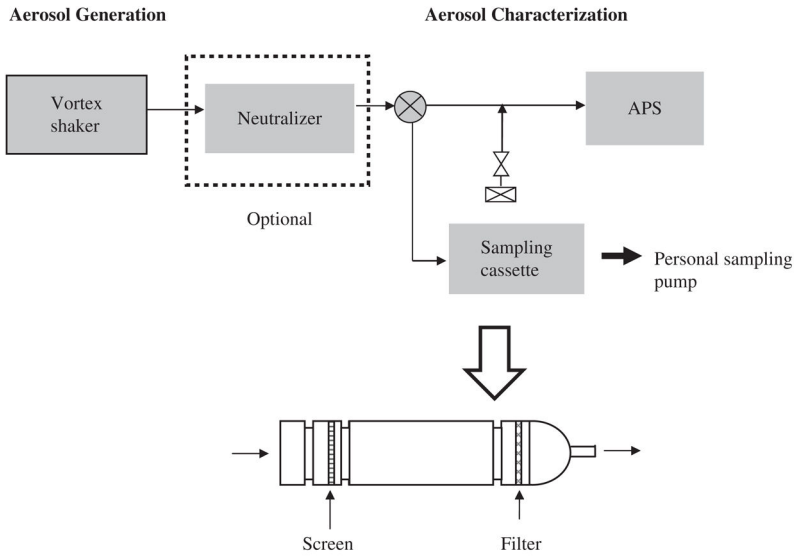

Figure 1.
Experimental setup for length measurement of fibers (top); configuration of a sampling cassette with a screen and a filter (bottom).

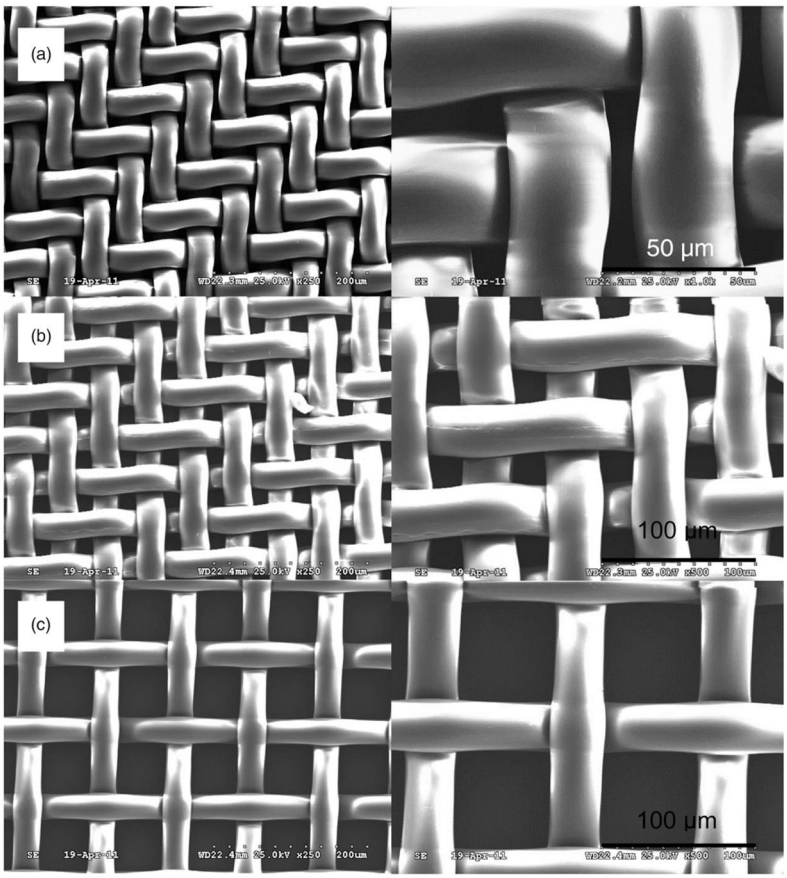

Figure 2.
SEM images of nylon mesh screens with different aperture sizes used in this study. (a) 10 µm, (b) 20 µm and (c) 60 µm mesh size.

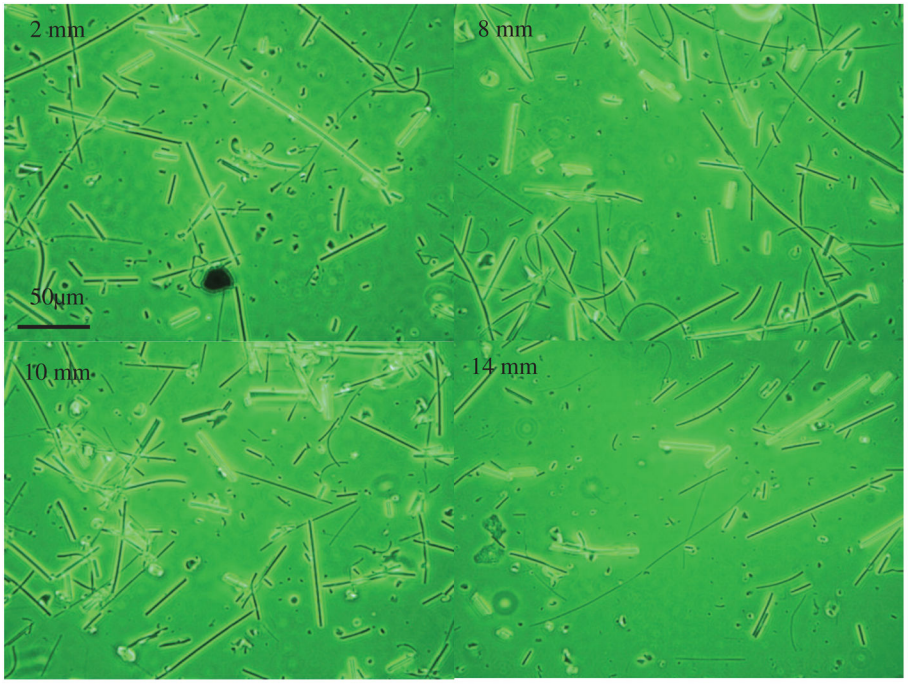

Figure 3.

Optical microscope images of the glass fibers aerosolized by vortex shaking and collected on MCE filter with no screen. The number at the top left is the distance from the location where the first fibers are visible on the far left of the MCE filter.

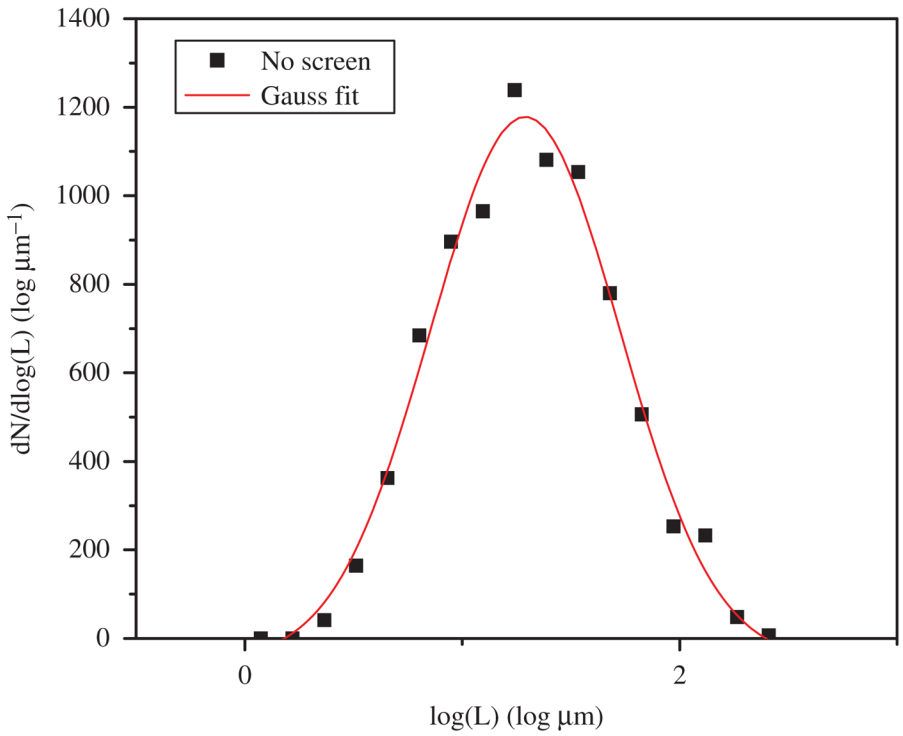

Figure 4.

Log-normal length distribution of the glass fibers aerosolized by vortex shaking and collected on MCE filter with no screen. The lengths of the fibers were measured using a phase contrast microscope.

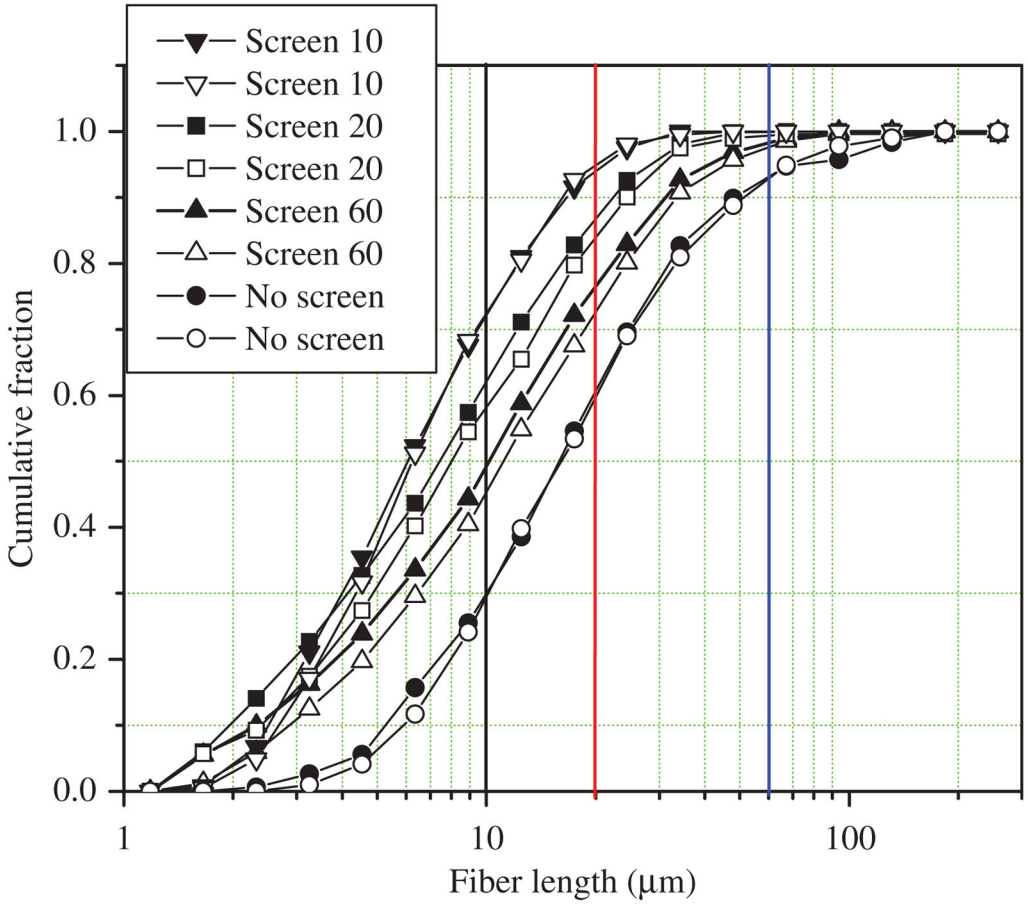

Figure 5.

Cumulative fractions of glass fibers penetrated through a screen and collected on MCE filter for different screen mesh sizes. The vertical lines at 10, 20 and 60 μm are included as indicators of the relevant screen apertures.

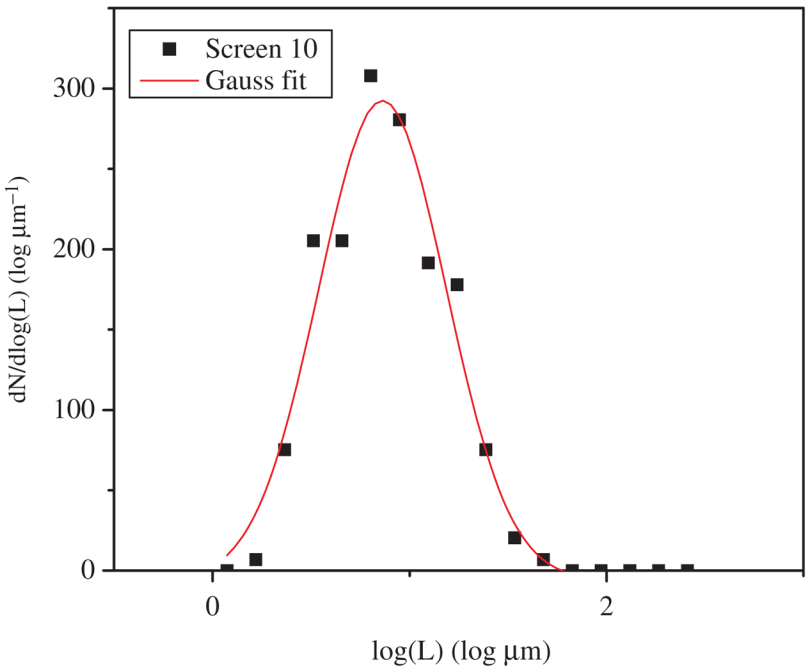

Figure 6.

Log-normal length distribution of the glass fibers aerosolized by vortex shaking and collected on MCE filter with screen 10. The lengths of the fibers were measured using a phase contrast microscope. The Gaussian fit yields a GML=7.47 and GSD=2.13.

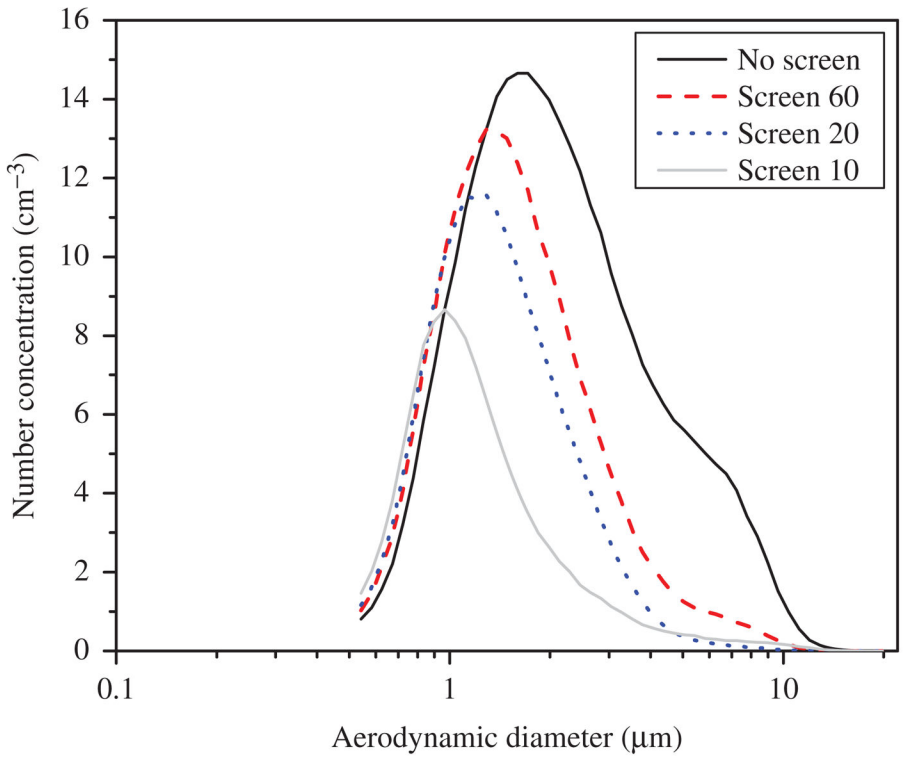

Figure 7.
Number concentration versus aerodynamic diameter of the glass fibers aerosolized by vortex shaking and measured by an aerodynamic particle size for different mesh size screens (10, 20 and 60 μm).

(a)

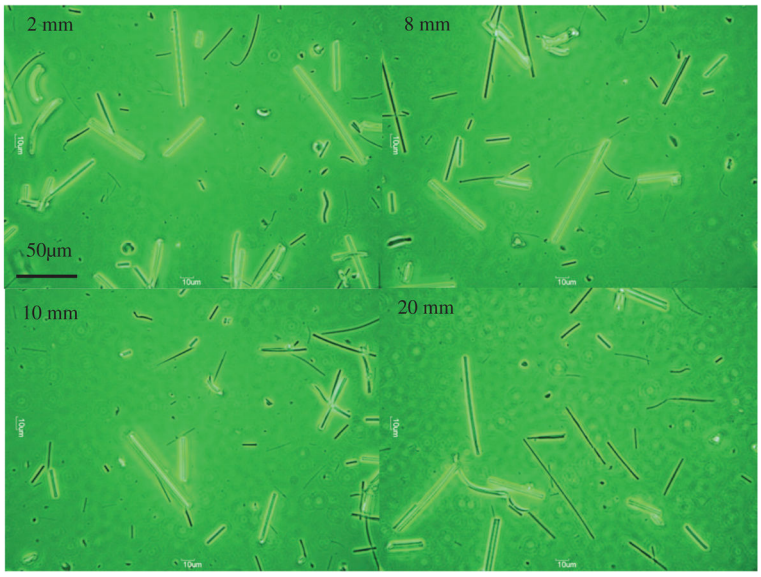

(b)

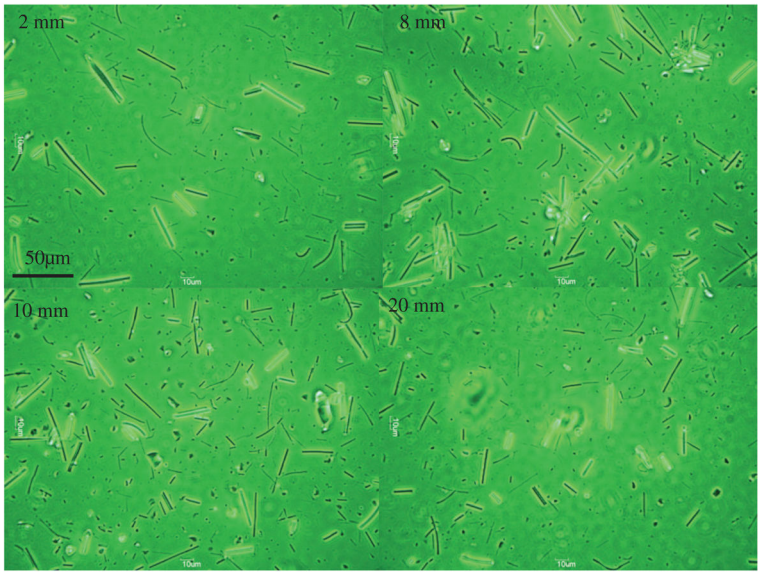

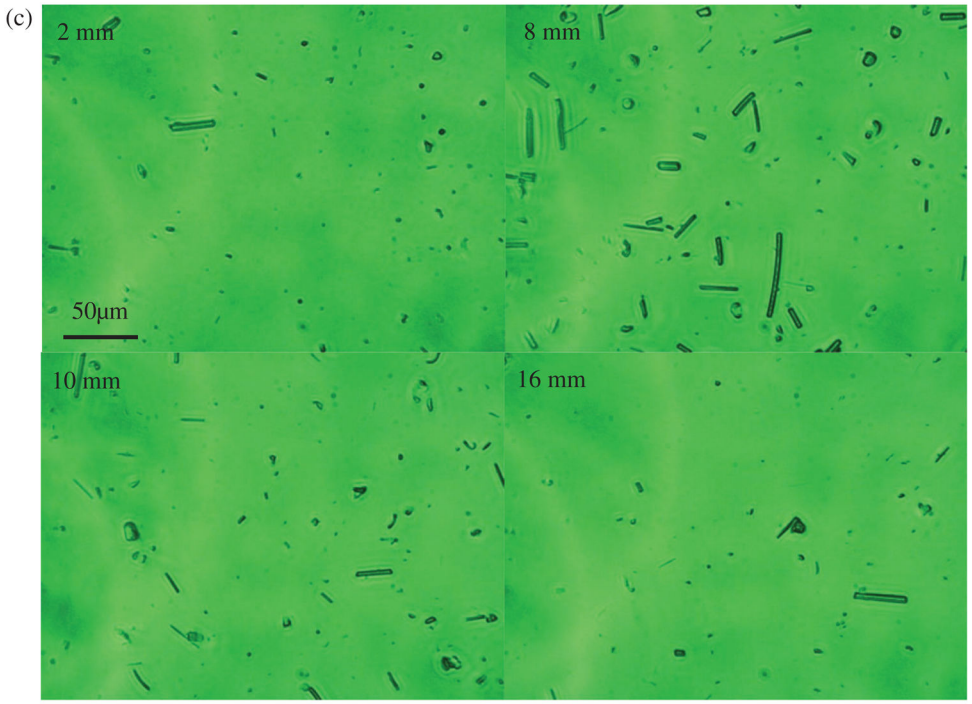

Figure 8.

Optical microscope images of glass fibers penetrated through a screen and collected on a 25mm MCE filter. The number on the left top is distance from the location where the first fibers are visible on the far left of the MCE filter. (a) 60 μm screen, (b) 20 μm screen, (c) 10 μm screen.

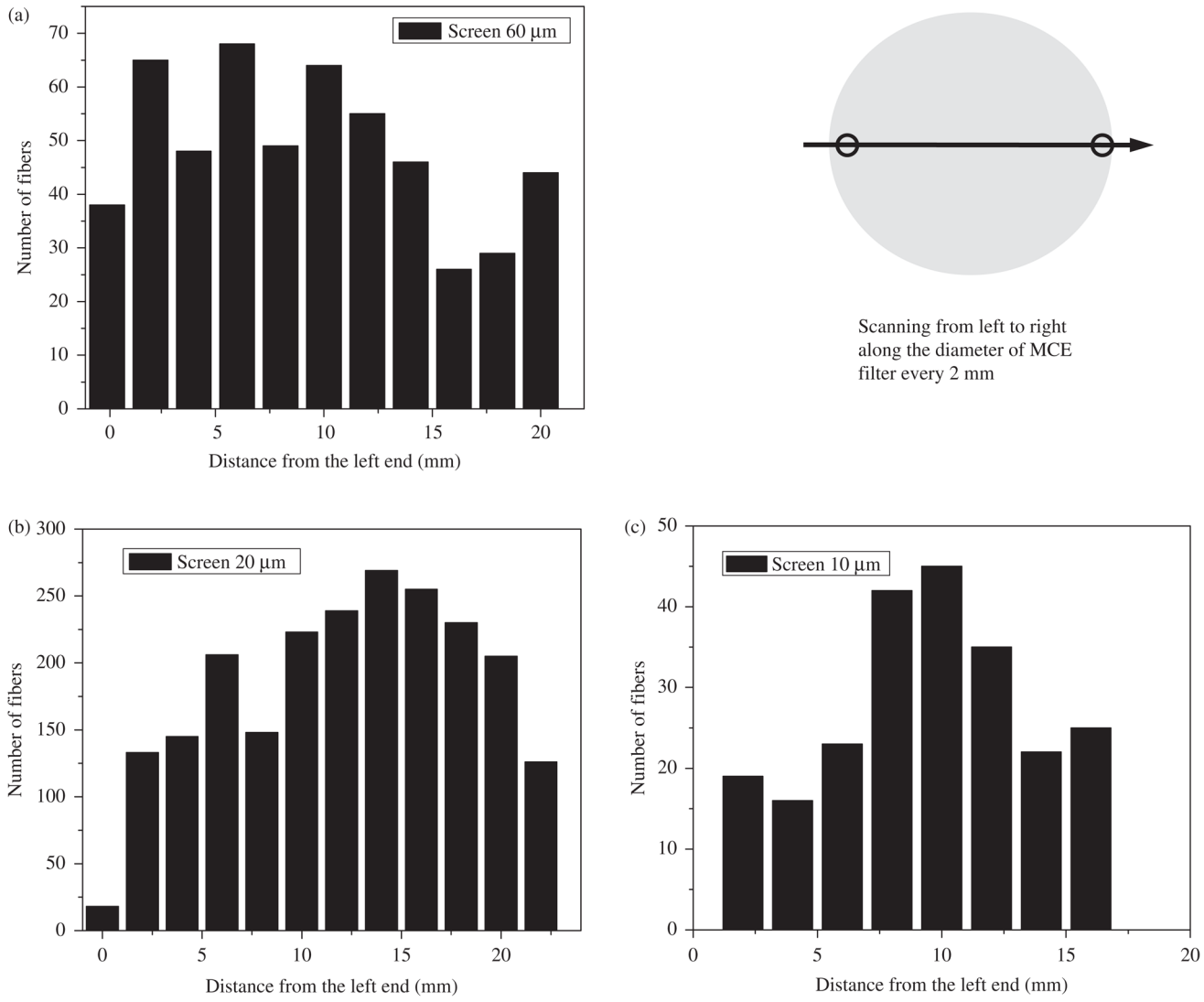

Figure 9.

Loading of fibers penetrated through each screen and collected on a 25mm MCE filter. (a) Screen 60, (b) screen 20 and (c) screen 10. Mean number of fibers counted on each field of view is 48, 183 and 28 for screens 60, 20 and 10, respectively.

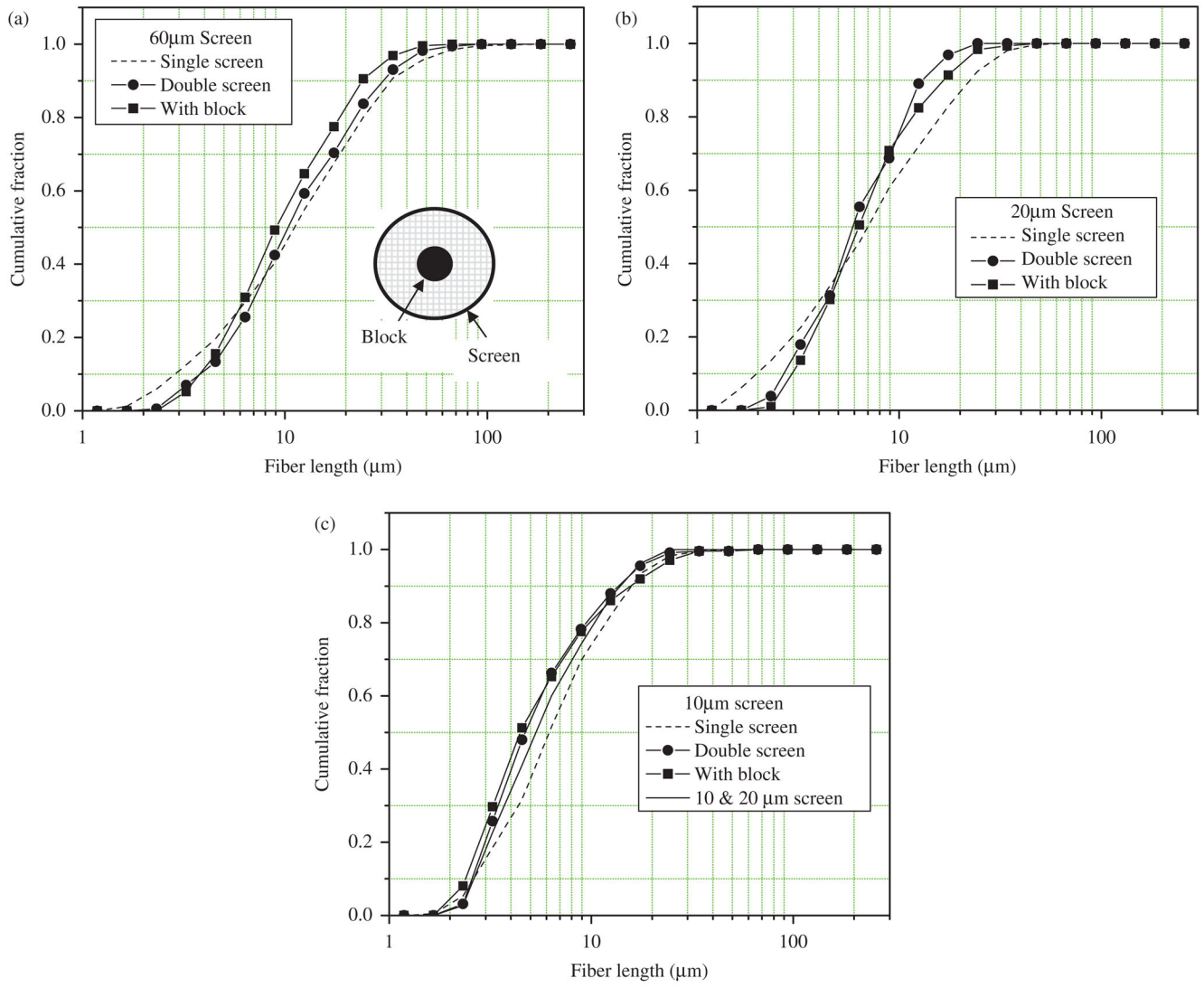

Figure 10.

Cumulative fractions of fibers penetrated through each screen with different configurations and collected on a 25mm MCE filter: (a) 60 µm screen; (b) 20 µm screen; (c) 10 µm screen. Fiber length distributions are constructed from PCM images taken at 40×. Inset (a): schematic diagram for the centrally blocked screen configuration.

Table 1

Geometric mean length, geometric standard deviation and number of fibers longer than 20 μm of length distributions of fibers penetrated through a screen for different mesh sizes.

Test condition	Geometric mean length (GML) [μm]	Geometric standard deviation (GSD)	Fraction [%] of fibers longer than 20 μm
No screen	18.3	2.31	40.0
No screen	18.4	2.41	40.9
Screen 60	12.3	2.80	23.9
Screen 60	13.3	2.92	27.9
Screen 20	8.67	2.99	13.6
Screen 20	9.82	2.78	16.5
Screen 10	7.14	2.30	6.3
Screen 10	7.47	2.13	4.8
Double Screen 60	12.0	2.43	24.8
Blocked Screen 60	10.8	2.26	17.8
Double Screen 20	7.19	2.00	2.0
Blocked Screen 20	7.19	1.94	6.1
Double Screen 10	5.20	1.78	3.2
Blocked Screen 10	4.82	1.79	6.2
Mixed Double Screen: 10 & 20	6.19	2.04	2.4

Fiber length distributions obtained from PCM images taken at 40× magnification.